analytical chemistry

Article

pubs.acs.org/ac

Dynamics Displayed by Energetic C_{60} Bombardment of Metal Overlayers on an Organic Substrate

Paul E. Kennedy,[†] Zbigniew Postawa,[‡] and Barbara J. Garrison*[,†]

[†]Department of Chemistry, 104 Chemistry Building, Pennsylvania State University, University Park, Pennsylvania 16802, United States

[‡]Smoluchowski Institute of Physics, Jagiellonian University, ul. Reymonta 4, 30-059 Kraków, Poland

Supporting Information

ABSTRACT: Cluster bombardments of 15 keV C_{60} on metal−organic interfaces composed of silver atoms and octatetraene molecules were modeled using molecular dynamics computer simulations. Dynamics revealed by the simulations include the formation of holes in the metal overlayers from which underlying organic molecules are sputtered predominantly by a rapid jetlike motion and the implantation of metal atoms and clusters in the underlying organic solid. Both of these processes negatively affect the information depth for cluster bombardment of metal−organic interfaces; therefore, the simulations presented here give a clear picture of the issues associated with depth profiling through metal−organic interfaces.

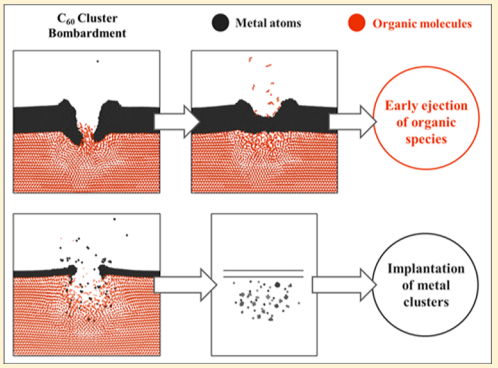

Three-dimensional characterizations of materials with depth resolutions down to the nanometer level can be obtained using time-of-flight secondary ion mass spectrometry (TOF-SIMS). Depth profiles can be produced by continuously bombarding the surface with cluster ions so that successive layers of the material are removed and analyzed by the TOF-SIMS instrument. Due to dynamic and chemical effects of the cluster ions' interaction with the surface, not all materials are easily or successfully depth profiled.[1−4] Samples that contain metal−organic interfaces are one type of material that has been shown to be particularly problematic.[2] Metal layers are important components in organic electronic devices. The most prominent example is the metal cathode in organic light-emitting diodes (OLED).[5] However, metal layers have also been applied in developing organic bistable devices for rewritable memory cells,[6,7] and in the construction of metal−organic microcavities,[8] which could be used to develop electrically driven organic solid-state lasers. The difficulty of depth profiling through metal−organic interfaces was shown by Cheng and Winograd for depth profiles of both aluminum overlayers on a peptide-doped trehalose film and Ag overlayers on a pure trehalose film using a C_{60}^+ ion beam.[2] In the depth profiles, the secondary ion signal for the metal species was shown to persist well below the metal−organic interface. The observed effects on the depth profiles were attributed to the possible mixing and chemical damage resulting from ion cluster bombardment. Recently, TOF-SIMS has been used successfully to depth profile through OLED type devices using large gas cluster ion beams with the caveat of having first removed the outer metal cathode or that the construction of the device did not include a metal cathode.[4,9,10] The necessity to remove the metal cathode is added evidence suggesting that there are complications when depth profiling through the metal−organic interfaces. Understanding the microscopic origin of these difficulties and finding practical solutions are, therefore, important.

Molecular dynamics (MD) simulations have been instrumental in developing our current understanding of the mesoscopic processes that occur during cluster bombardment of both inorganic and organic solids.[11−22] Therefore, their application to the study of cluster bombardment of metal−organic interfaces is natural and should enable elucidation of the reasons for the difficulties of depth profiling through such systems. Recently, MD simulations performed by Restrepo et al. have been used to explain the enhanced sputtering yields observed in SIMS experiments on organic surfaces coated with metallic nanoparticles, a technique referred to as metal-assisted SIMS (MetA-SIMS).[23−25] The systems that the authors studied were composed of ∼2.5 nm gold nanoparticles (Au-NP) deposited on top of both crystalline and amorphous polyethylene (PE) surfaces or embedded in the amorphous PE. These studies show the complexity and diversity of actions that occur in systems with interfaces between metallic structures composed of heavy atoms and softer and lighter organic materials.

The objective of this paper is to describe the dynamics of energetic C_{60} cluster bombardment of metal overlayers deposited on an organic substrate. To accomplish this goal,

Received: November 19, 2012
Accepted: January 9, 2013
Published: January 9, 2013

   dx.doi.org/10.1021/ac303348y | *Anal. Chem.* 2013, 85, 2348−2355

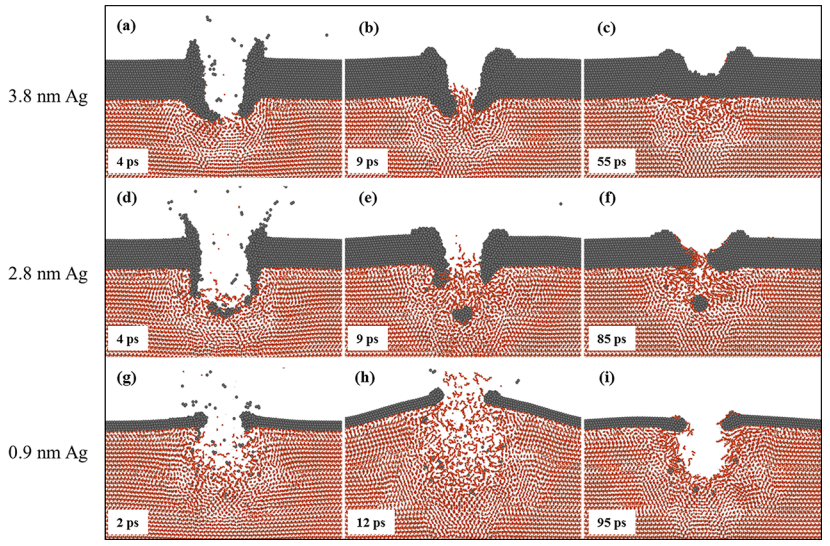

Figure 1. Cross-sectional snapshots of 15 keV 0° C_{60} bombardment of octatetraene crystalline solids (red) with varying thicknesses of Ag overlayers (gray, thicknesses listed on left). Frames are taken from 1.5 nm slices of the central part of the systems. Columns from left to right show different stages of the bombardment process, from the initial opening of a hole in the Ag overlayers, followed by a plume of ejected organic material, and finally the resulting topography from the C_{60} impact.

MD simulations of 15 keV C_{60} bombardment at normal incidence of silver (Ag) metal overlayers with a thickness varying from 0 nm (a bare octatetraene crystal) up to 4.7 nm on a crystalline octatetraene substrate have been performed. The results are used to provide insight into phenomena being responsible for the difficulties associated with depth profiling through metal−organic interfaces.

DESCRIPTION OF THE CALCULATION

Molecular dynamics simulations were employed to investigate the dynamics of cluster bombardment of metal−organic interfaces. Ag{111} and a *trans,trans*-1,3,5,7-octatetraene crystal (C_8H_{10}) were chosen for the metal overlayer and underlying organic solid due to previous familiarity with using these systems in MD simulations.[19,26−28] Systems with metal overlayers varying from 4.7 nm thickness down to the bare octatetraene solid in roughly 0.94 nm (four atomic layers) decrements were utilized to mimic the various stages of transition through a metal−organic interface during depth profiling. The crystalline octatetraene solid has a monoclinic structure with a density of 1 g/cm^3,[29] which is much smaller than a density of 10.5 g/cm^3 for a face-centered cubic (fcc) Ag sample. There is also a significant difference in cohesive energies between these materials. Octatetraene and silver have cohesive energies of 0.52 and 2.95 eV, respectively. The CrystalMaker program was used to generate the octatetraene structure,[30] which was then energy minimized. Thirty-five layers of Ag{111} were positioned above the organic surface, and the system was allowed to quench. The resulting system was then cropped into hemispheres with the appropriate radius to confine 15 keV of the primary kinetic energy for the intended metal overlayer thickness. As a result, the radius of the hemispherical samples changed from 16.5 nm for a thickest metal overlayer to 20.5 nm for the bare molecular crystal. Corresponding samples have from 709 011 to 1 854 312 atoms. Excluding the surface, the outer shell of the hemispherical systems were contained by a rigid boundary of 1.3 nm, which was bordered by a stochastic region with a width of 2.6 nm that was used to prevent reflection of the pressure waves generated by the cluster impacts.

Several interatomic potentials were used to model the relevant interactions that occur during the bombardment process. The reactive AIREBO potential was used for interactions between the hydrocarbon atoms comprising both the molecules of the octatetraene solid and the C_{60} cluster.[31] The Ag−Ag interactions were described by the molecular dynamics/Monte Carlo corrected effective medium (MD/MC-CEM) potential.[32] Because a potential that would describe chemistry between the Ag and the organic molecules does not exist, interactions between Ag and organic atoms were described using two-body Lennard-Jones (LJ) potentials splined with Moliere potentials for the repulsive walls.[33] The parallel sputtering code implementing the message passing interface strategy (MPI) was used to perform calculations. The details of this approach can be found elsewhere.[34] We used 16 processors per simulation, and the elapsed time per trajectory ranged from 1 to 6 weeks. We used a variable time step fifth-order Gear predictor−corrector integrator,[34] and the time step ranged from hundredths of femtoseconds, during the initial impact of the cluster when the forces are changing most rapidly, to a little over one femtosecond at the end of the trajectory. Simulations were terminated when molecular sputtering from the organic solid had ceased, which usually took from 50 to 90 ps. Since the goal is to understand the general dynamics of the bombardment of a metal/organic system and not to obtain detailed quantitative results, we have calculated only one trajectory per set of initial conditions.

The simulations described here stretch the use of empirical interaction potentials. As we have noted previously,[11,34−37] if one does not have a perfect set of interaction potentials, then that limits the interpretations that can be made from the computer simulations. Briefly, the reactive REBO potential has been described quantitatively for small molecules and fragments by Brenner et al.[38,39] The energetics and geometry of small molecules such as octatetraene are well-described; however, the quantitative descriptions of activation barriers for reactions other than direct bond cleavage are not calibrated and there is

dx.doi.org/10.1021/ac303348y | *Anal. Chem.* 2013, 85, 2348−2355

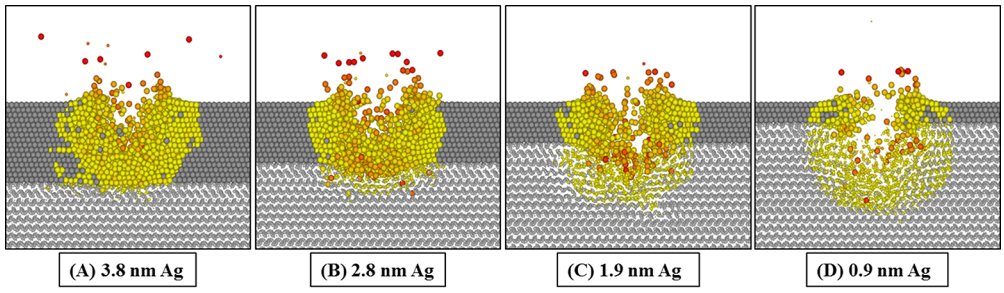

Figure 2. 1.5 nm cross sections of C_{60} cluster impacts of Ag/octatetraene systems at 400 fs colored according to an atom's kinetic energy (yellow to red 0.1−20 eV, gray <0.1 eV, where dark gray are Ag atoms and light gray are C and H atoms). The kinetic energy totals for the Ag and octatetraene regions for each of the different systems shown are (A) 9.6 and 0.4 keV, (B) 10.6 and 0.8 keV, (C) 8.0 and 2.6 keV, and (D) 3.6 and 5.5 keV, respectively.

no reason to suspect that the reaction barriers are good. The long-range portion of the AIREBO potential[31] has been described by its authors. The binding energy of the octatetratene crystal is experimentally unknown. The experimental octatetraene structure is stable using the AIREBO potential. The interaction between the Ag surface and atoms with the organic molecules and fragments is a complete approximation because, unfortunately, there is not a good many-body description for the system. The LJ potential used describes a weak interaction between particles. In summary, then, the system described in the simulation is a molecular solid bound weakly to a metal overlayer. The results that we can describe well are those related to physical processes such as changes in ejection mechanism and how the change in mechanisms changes the sputtering yield and kinetic energy distribution. There is limited ability to describe specifics of chemical reactions. Moreover, we view this system as a generic molecular solid with a generic metal overlayer and do not attach significance to the octatetraene and Ag chemistry.

The empirical potentials generally used assume that the system stays in the ground electronic state. Consequently, all bond cleavage reactions go to neutral species and not ionized states. Also, as discussed previously[40] the impact of the cluster can create a very dense region in molecular solids. This environment cannot be described by a single electronic state. Thus, the initial reactions in the systems in which the cluster deposits considerable energy in the organic material should be considered approximate.

RESULTS AND DISCUSSION

Distinctive dynamics are elucidated by MD computer simulations for the energetic cluster bombardment of systems composed of metal overlayers on an organic substrate as compared to the energetic cluster impacts on systems such as inorganic solids, molecular organic solids, molecular organic overlayers on metal substrates, and metal nanoparticles deposited on organic polymer substrates.[11,20,25,41−48] Important factors responsible for these distinctive dynamics include the large disparity in the cohesive energy of the tightly bound metal atoms in the overlayer and the loosely bound organic molecules of the substrate and the much greater compressibility of the organic material compared to the metal overlayer. The resulting dynamics due to kiloelectronvolt cluster bombardment depends on the metal overlayer thickness as shown in Figure 1.

The MD studies performed on single-component systems have shown that the basic dynamics initiated by C_{60} impact involve projectile-stimulated mesoscopic motion that pushes material hemispherically away from the impact point. The lateral movement of relocated material is later converted into vertical fluid-like motion of atoms along the walls of the forming crater. The downward motion of material causes the material below the impact point to compress. This compressed material eventually relaxes and causes an upward movement of atoms to fill in the bottom of the crater.[19,21,26,49,50] The final result of all these actions is the formation of the azimuthally isotropic crater surrounded by the almost circular rim. Atoms or molecules with sufficient kinetic energy can escape the surface and be ejected. MD studies identify two processes leading to particle emission. High-energy particles are emitted from the forming corona of the crater soon after the projectile impact by a fluid flow type process, while low-energy particles are ejected later from the volume of the crater by an effusive-like motion.[49] Although these basic motions are also observed for these metal−organic overlayer systems as shown in Figure 1, there are also important differences. The snapshots for each system of Figure 1 are taken at the moment when the metal overlayer is penetrated by the C_{60} cluster (left), when a plume of ejecting organic molecules and fragments initiates (middle), and when the final surface topography is formed (right). First, for the 3.8 nm film (Figure 1a−c and Animation 1 in the Supporting Information), the main change from the pure metal system is that the soft organic material allows the metal layer to push into it creating a small but temporary hole. Some of the organic molecules expand into the hole (Figure 1b) and eject, while some ultimately adsorb to the top metal surface. In this case, almost all impacting energy is absorbed in the metal overlayer (see caption to Figure 2). The trend continues for the 2.8 nm film (Figure 1d−f and Animation 2 in the Supporting Information) except that now the thickness of metal layer is not sufficient to absorb all the incident energy, integrity of the layer is compromised, a permanent hole in the overlayer is created, and chunks of metal are deposited in the organic material. Organic molecules eject through the hole, and organic material coats the metal surface as shown in Figure 1f. The final configuration includes one large metal cluster and several metal atoms deposited in the organic layer. For the 0.9 nm film (Figure 1g−i and Animation 3 in the Supporting Information) the C_{60} blasts into the organic substrate depositing many metal particles into the organic material. Much of the cluster energy is deposited in the organic layer. If there were no overlayer, the organic molecules would begin to flow off the surface by the fluid flow along the walls of the forming crater.[28,49] The metal overlayer, however, prevents this type of ejection. The upward motion of the molecules is blocked by the overhanging metal

dx.doi.org/10.1021/ac303348y | Anal. Chem. 2013, 85, 2348−2355

layer, and the pressure exerted by the organic molecules trying to escape puts the thin metal layer into a cantilever-type motion (see Animation 3 in the Supporting Information). The existence of the hard metal overlayer limits the diameter of the crater opening as compared to the bare organic solid making it more difficult for the molecules to eject. The final topography of the system depicted in Figure 1i is of a crater 4 nm deep with the metal overlayer overhanging the crater walls of the organic region. Even though a few metal clusters were sputtered with the upward expansion of solid, the majority of these clusters remain implanted in the organic region (Figure 1i).

Energy Deposition. How the C_{60} energy is deposited illustrates the mechanisms of damage formation and sputtering. Snapshots of the kinetic energy distribution taken at 400 fs, a time when the energy has reached the interface for all layer thicknesses, are shown in Figure 2A–D. The atoms are colored by their kinetic energies with gray atoms indicating energies less than 0.1 eV and atoms with from 0.1 to 20 eV of kinetic energy colored from yellow to reddish orange. Particles with greater than 20 eV are red. The discussion below focuses on the red atoms. The caption gives the total kinetic energy deposited in both the metal overlayer and the organic substrate for the given systems.

The starting point for understanding the change in the energy deposition as a function of metal layer thickness is for the thickest layer as shown in Figure 2A. The energy that goes into the metal substrate is distributed among many Ag atoms as the hard metal material is relatively uncompressible. In this case, almost 96% of deposited energy is confined to the metal overlayer. When the metal overlayer is thinner (Figure 2, parts B and C), the energy deposition occurs both in the metal and organic layers. There are two consequences of this change. First, there is energy directly deposited in the organic layer that goes toward ejecting molecules or remains trapped in the organic substrate leading to material mixing. Second, metal atoms move downward at the interface and are deposited in the organic material. Solid metal samples, on the other hand, confine the energy deposition to a depth of about 4 nm; the introduction of a metal–organic interface allows the energy as well as metal particles to go as deep as 8 nm below the surface as seen in Figure 1 and discussed below. The change in the mechanism of energy transfer as the metal overlayer becomes thinner affects the amount and spread of metal implantation in the organic substrate as well as the velocities of the sputtered organic molecules.

Kinetic Energies of Sputtered Substrate Molecules. A change in the mechanisms of ejection stimulated by cluster impacts on systems with metal overlayers with respect to cluster impacts on pure organic solids is reflected in the kinetic energy (KE) distributions of sputtered substrate molecules shown in Figure 3. The KE distribution for the molecular solid is characterized by an initial rise from 0 eV to a peak at about 0.4 eV followed by a decay at higher energies. One could expect that molecules ejected from metal-covered systems would have a lower kinetic energy as a large portion of the primary energy is absorbed in the metal overlayer. The distributions of the kinetic energy of sputtered molecules from the systems with metal overlayers, however, are shifted to higher KE as compared to bare organic solid. In fact, there are very few molecules sputtered with kinetic energy below 1 eV, while over 40% of the molecules sputtered from the pure organic solid have kinetic energies less than 1 eV. As already mentioned, in

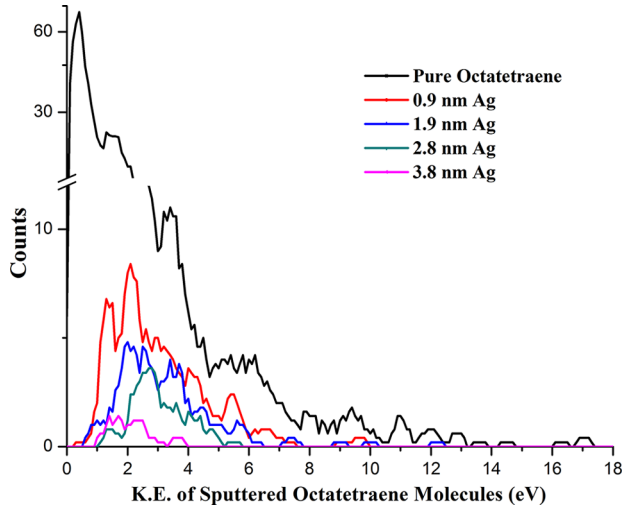

Figure 3. Kinetic energy distributions of sputtered octatetraene molecules for different overlayer thicknesses.

bare organic solids molecules with high kinetic energy are ejected relatively soon after projectile impact from the corona of the forming crater by a fluid flow process, while low-energy molecules are emitted later from the volume of the crater by effusion.[28,49] Our data indicate that low-energy emission is hindered due to existence of a thick metal channel with relatively narrow diameter that is formed in the punctured metal overlayer. Animations of the cluster bombardment also show that the fluid flow mechanism leading to emission of high-energy molecules from the corona of the crater is absent due to blocking of the molecular flow by the dense metal overlayer composed with heavy atoms bounded with high cohesive energy. This observation indicates that high-energy molecules must be ejected by some other mechanism not present during sputtering of pure organic systems.

This mechanism of emission can be identified from the available animations of the cluster impacts that show that the hole produced in the metal overlayer as well as the bending of this layer into the organic material by the impacting cluster causes a jetting effect in the upward flow of substrate molecules from a pressurized volume located below. As a result of the jetting, the organic molecules experience an increase in velocity as they eject into vacuum. In addition, the forward peaked angles of emission can clearly be seen in the animations. This jetting effect may become more pronounced as the metal overlayer thickness increases since the cross-sectional area of the hole is decreasing and a higher pressure is needed to squeeze the molecules out. This is indeed observed for the 0.8, 1.9, and 2.8 nm overlayers. However, as the layer becomes too thick it absorbs most of the primary energy, and at certain moment, the delivered energy is too small to enhance sufficient pressure and the process of jetting disappears. Such is the case for the overlayer 3.8 nm as indicated by the kinetic energy distribution shift to lower kinetic energies as compared to thinner metal overlayers.

Sputtering Yields. The creation of holes in the metal overlayer due to the cluster bombardment followed by the jetting of the organic molecules from the organic substrate means that the sputtering yield of molecules initiates at a metal layer coverage of 3.8 nm as shown in Figure 4 and steadily increases as the metal thickness decreases. For the organic solid (i.e., no metal overlayer), the yield is 4.5 times larger than for

dx.doi.org/10.1021/ac303348y | Anal. Chem. 2013, 85, 2348–2355

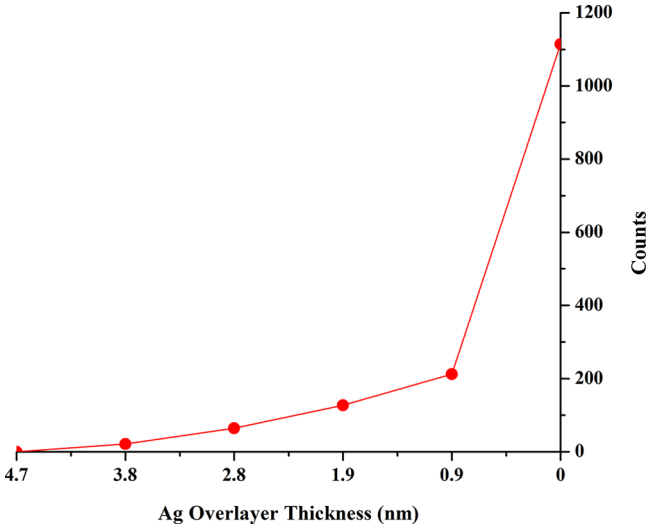

Figure 4. Total sputtering yield of octatetraene molecules vs metal overlayer thickness.

the 0.9 nm overlayer, which indicates that even a thin overlayer has a pronounced influence on molecular emission. The metal overlayers thus suppress the molecular yield. As discussed above, the most prominent mechanism of emission with the metal overlayer is jetting motion, whereas the emission from an uncovered surface is through fluid flow and effusion.[28,49]

The sputter yield trend with respect to Ag overlayer thickness from Figure 4 is in line with the experimental results found by Cheng and Winograd for depth profiles of a 15 nm Ag overlayer on a 650 nm thick film of trehalose sugar using a 20 keV C_{60}^+ primary ion beam at 40° angle of incidence.[2,51] The depth profiles show the rise of the trehalose signal starting at roughly halfway through the erosion of the Ag film and continuing to rise through the Ag–trehalose interface. Early onset of the trehalose signal indicates the penetration of the Ag overlayer and escape of trehalose well before the interface has been reached. The formation of holes in the Ag overlayers shown in Figure 1 depicts how this is possible. Also, the increase in the sputtered molecules with decreasing Ag overlayer thickness, shown in Figure 4, agrees with the increase in the trehalose signal as it approaches the Ag–trehalose interface. Of course, the trehalose depth profile shows the penetration of a much thicker Ag overlayer than was used in the simulations; however, the experimental C_{60}^+ beam was at a higher kinetic energy, and the Ag surface had already been eroded, which would have resulted in a roughened surface that could have regions much thinner than the ~7.5 nm Ag penetration that the depth profile would imply.

Mixing by Metal Cluster Implantation of the Organic Substrate. The energetic cluster impact leads not only to ejection of Ag particles but also causes implantation of the metal atoms into the organic substrate. The results of the implantation of metal clusters in the organic substrate for three different metal overlayer thicknesses are shown in Figure 5. A

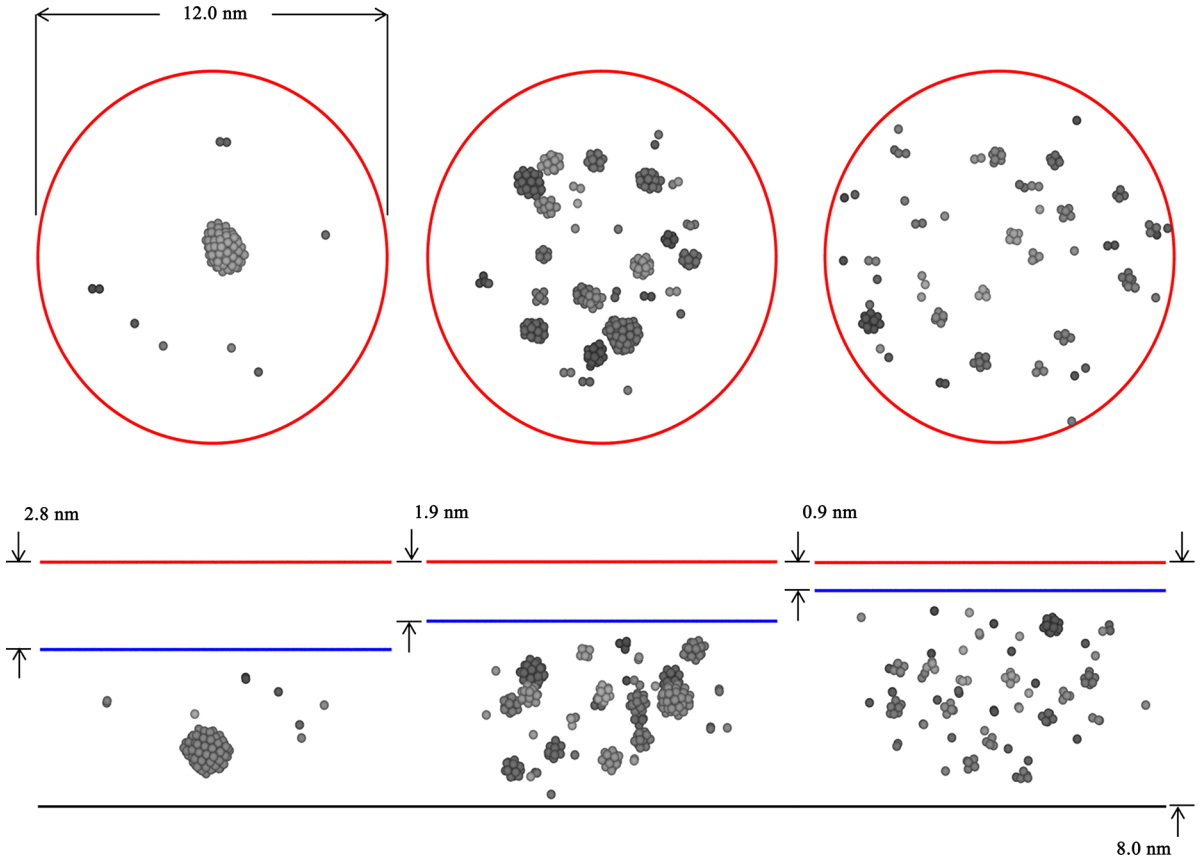

Figure 5. Images showing the amount, size, and distribution of Ag clusters implanted in the octatetraene substrate of the solid for a given metal overlayer thickness. Top row of images shows a view looking down on the sample from the direction of C_{60} cluster impact. Bottom row is the side view. The red line indicates the original surface height, and the blue line represents the Ag–octatetraene interface; the solid black line is the depth at 8 nm. Ag atoms are depth-cued so that light gray atoms are closest to the viewer and dark gray the farthest away.

dx.doi.org/10.1021/ac303348y | *Anal. Chem.* 2013, 85, 2348–2355

top view of the horizontal spread of the metal clusters is presented in the top of the figure, and a side view showing the depth of the implanted clusters is shown in the bottom of the figure with the red line indicating the original surface height and the blue line indicating the initial interface between the metal overlayer and the organic substrate. The images in both the top and bottom of Figure 5 clearly show that, as the metal overlayer thickness decreases, the size of the implanted clusters is reduced and the lateral and vertical spread in the implanted clusters increases. As can be seen by the darker orange and red metal atoms in Figure 2, parts C and D, the kinetic energies of the metal clusters, that break free of the metal overlayer, increase as the metal overlayer thickness decreases. The increase in KE of the metal cluster and the decrease of the average cluster size translate into the faster clusters and thus is the cause of the increase in the spread of the metal clusters as the overlayer thickness decreases.

Experimental depth profiles of a 15 nm Ag overlayer on a 650 nm thick trehalose film show that the Ag signal monotonically decreases, yet persists, through the extent of the trehalose film thickness.[2] The implantation of metal clusters shown in Figure 5 demonstrates why initially, after reaching the Ag−trehalose interface, the Ag signal is being detected since the metal clusters have been implanted roughly 8 nm deep in the substrate and would have to be sputtered after the Ag overlayer has been removed. However, the persistence of the Ag signal through 650 nm of trehalose implies that the C_{60} cluster's ability to clean up the damage incurred by penetrating the metal overlayer is being impaired. The larger size metal clusters produced by cluster impacts on thicker overlayers, as seen in Figure 5, could fragment on subsequent cluster impacts resulting in metal clusters driven deeper into the substrate. Also, smaller metal clusters could undergo interlayer mixing within the organic substrate during multiple cluster bombardment. It is plausible that the combination of these phenomena could result in the continuation of signal from the metal overlayer through the organic substrate that was seen in the depth profiling experiment.[2]

Depth Profiling through Metal−Organic Interfaces. The calculations presented herein yield perspective into why depth profiling through a metal−organic interface such as found in an OLED is challenging. Molecular dynamics simulations of repetitive bombardment of a Ag surface[18,52−55] along with a model[56,57] to extrapolate the MD results to actual depth profiles have allowed us to identify two key features important for good depth profiles.

First, the information depth or depth from which particles are sputtered should be small. The information depth has two components, the inherent depth from which material is sputtered convoluted with the peak-to-valley height associated with the root mean square (rms) roughness. At this point we cannot compare rms roughness of this system with the metal Ag system for which we have performed repetitive bombardment simulations; thus, we stick to comparing the depth from which particles sputter. For Ag, the typical sputter depth is ∼2.5 nm as shown in Figure 1c. The crater depth for the pure organic material is also about 2 nm. If we take the 2.8 nm film of Figure 1d−f as our example overlayer since it is just slightly thicker than the pure material information or sputter depths, we can see from Figure 1e that organic molecules from 3 to 4 nm below the surface are ejecting. Thus, the information depth for the organic molecules is greater in the metal−organic interface region for the flat surface of either pure organic or pure metal.

Second, the amount of material displacement due to the cluster's impact should be small for good depth profiles. For the metal system,[58] the displacements for a single impact are dominated by up and down motions of 1 nm although there is some contribution of 2 nm movements up and down. From Figure 1, parts f and i, organic molecules can have upward displacements of 1−3 nm due to the jetting effect. From Figure 5, metal atoms can have downward displacements of 3−6 nm. These particles will collide with organic molecules causing additional relocation. As a result, the average material relocation is significantly increased when the metal−organic interface is reached.

The snapshots of the systems taken after bombardment suggest the presence of an additional complexity for depth profiling through a metal−organic interface, namely, a changing environment. The pictorial information shown in Figures 1 and 5 clearly show that subsequent impacts will see not only a different surface topography but also a different environment, one with holes in the metal overlayer, metal atoms and clusters of metal atoms in the organic layer, and organic molecules on top of the metal overlayer. The MD simulations of Restrepo et al.[23−25] show very clearly that the microscopic nature of the impact environment with nanoparticles in an organic matrix can have a significant influence on the dynamics. In addition, depending on the particular combination of species, the physical mixing of metal atoms with intact molecules and fragments of molecules could induce chemical changes in the system and, consequently, may significantly modify the ejection yield of secondary ions as was observed in MetA-SIMS experiments.[59−63]

The larger information depth, the larger displacements, and the altered physical and chemical environment provide a glimpse into why depth profiling through a metal−organic interface is challenging. The real issue, however, is whether the insight obtained from these simulations aids in designing a better strategy for depth profiling through a metal−organic interface. First, any layer with a low cohesive energy (large volatility) below a layer with large cohesive energy will present a challenge because holes can open in the overlayer and energy can get trapped in the underlayer forming separated, highly pressurized volumes that extend deep into the solid from where molecules will be released in a jetting motion. The next challenge is to prevent the metal atoms from implanting in the organic substrate. The ease with which the metal atoms implant is in part due to the mass mismatch between the metal atoms and the carbon and hydrogen atoms in the organic material. The light elements have difficulty in efficiently stopping the heavier atoms. The other challenge is that, at least in the case considered here, the organic material is much more compressible than the metal overlayer. Any cluster that can sputter the metal will also push it into the organic layer. Reduction of the impacting cluster's kinetic energy to the point where metal atoms are no longer being implanted in the organic layer will result in inconsequential sputtering thus terminating the depth profiling process. These factors arise from the inherent system properties and cannot be altered experimentally.

CONCLUSION

The dynamics associated with 15 keV C_{60} cluster bombardment of metal−organic interfaces consisting of Ag overlayers on an octatetraene organic solid were investigated using MD simulations. The impacting clusters were shown to create

holes in the metal overlayer through which the underlying organic molecules can sputter in a jetting motion. For metal overlayers thinner than 3 nm, metal atoms and clusters were implanted in the underlying organic solid. The larger information depth, the larger displacements, and the altered physical and chemical environment are the main reasons for the poor ability to depth profile through a metal−organic interface. Although the simulations provide a picture of the issues associated with depth profiling through a metal−organic interface, they do not provide a magic solution that will be under the experimentalist's control. We did perform test simulations with other beam conditions, for instance, with Ar_{872} clusters as the projectile. These simulations did not find a good solution.

■ ASSOCIATED CONTENT

Supporting Information

Animations as noted in the text. This material is available free of charge via the Internet at http://pubs.acs.org.

■ AUTHOR INFORMATION

Notes

The authors declare no competing financial interest.

■ ACKNOWLEDGMENTS

The authors gratefully acknowledge financial support from the National Science Foundation Grant No. CHE-0910564 and the Polish National Science Center Program No. PB1839/B/H02/2011/40. Computational resources were provided by the Research Computing and Cyberinfrastructure group at Penn State University.

■ REFERENCES

(1) Mahoney, C. M. *Mass Spectrom. Rev.* **2010**, *29*, 247.
(2) Cheng, J.; Winograd, N. *Appl. Surf. Sci.* **2006**, *252*, 6498.
(3) Cramer, H. G.; Grehl, T.; Kollmer, F.; Moellers, R.; Niehuis, E.; Rading, D. *Appl. Surf. Sci.* **2008**, *255*, 966.
(4) Niehuis, E. In *ToF-SIMS: Surface Analysis by Mass Spectrometry*, 2nd ed.; Vickerman, J. C., Briggs, D., Eds.; IM Publications: Chichester, U.K., 2012.
(5) Fu, H.; Cheng, Y.-M.; Chou, P.-T.; Chi, Y. *Mater. Today* **2011**, *14*, 472.
(6) Ma, L. P.; Liu, J.; Yang, Y. *Appl. Phys. Lett.* **2002**, *80*, 2997.
(7) Chu, C. W.; Ouyang, J.; Tseng, J.-H.; Yang, Y. *Adv. Mater. (Weinheim, Ger.)* **2005**, *17*, 1440.
(8) Brueckner, R.; Zakhidov, A. A.; Scholz, R.; Sudzius, M.; Hintschich, S. I.; Froeb, H.; Lyssenko, V. G.; Leo, K. *Nat. Photonics* **2012**, *6*, 322.
(9) Ninomiya, S.; Ichiki, K.; Yamada, H.; Nakata, Y.; Seki, T.; Aoki, T.; Matsuo, J. *Rapid Commun. Mass Spectrom.* **2009**, *23*, 3264.
(10) Ninomiya, S.; Ichiki, K.; Yamada, H.; Nakata, Y.; Seki, T.; Aoki, T.; Matsuo, J. *Surf. Interface Anal.* **2011**, *43*, 95.
(11) Garrison, B. J.; Postawa, Z. *Mass Spectrom. Rev.* **2008**, *27*, 289.
(12) Aoki, T.; Matsuo, J. *Nucl. Instrum. Methods Phys. Res., Sect. B* **2005**, *228*, 46.
(13) Aoki, T.; Matsuo, J. *Nucl. Instrum. Methods Phys. Res., Sect. B* **2007**, *261*, 639.
(14) Krantzman, K. D.; Wucher, A. *J. Phys. Chem. C* **2010**, *114*, 5480.
(15) Ryan, K. E.; Russo, M. F.; Smiley, E. J.; Postawa, Z.; Garrison, B. J. *Appl. Surf. Sci.* **2008**, *255*, 893.
(16) Russo, M. F., Jr.; Garrison, B. J. *Anal. Chem.* **2006**, *78*, 7206.
(17) Webb, R. P.; Garrison, B. J.; Vickerman, J. C. *Surf. Interface Anal.* **2011**, *43*, 116.
(18) Russo, M. F.; Postawa, Z.; Garrison, B. J. *J. Phys. Chem. C* **2009**, *113*, 3270.
(19) Postawa, Z.; Czerwinski, B.; Szewczyk, M.; Smiley, E. J.; Winograd, N.; Garrison, B. J. *J. Phys. Chem. B* **2004**, *108*, 7831.
(20) Postawa, Z.; Czerwinski, B.; Winograd, N.; Garrison, B. J. *J. Phys. Chem. B* **2005**, *109*, 11973.
(21) Anders, C.; Bringa, E. M.; Fioretti, F. D.; Ziegenhain, G.; Urbassek, H. M. *Phys. Rev. B* **2012**, *85*, 235440.
(22) Smiley, E. J.; Winograd, N.; Garrison, B. J. *Anal. Chem.* **2007**, *79*, 494.
(23) Restrepo, O.; Prabhakaran, A.; Hamraoui, K.; Wehbe, N.; Yunus, S.; Bertrand, P.; Delcorte, A. *Surf. Interface Anal.* **2010**, *42*, 1030.
(24) Restrepo, O. A.; Delcorte, A. *Surf. Interface Anal.* **2011**, *43*, 70.
(25) Restrepo, O. A.; Prabhakaran, A.; Delcorte, A. *Nucl. Instrum. Methods Phys. Res., Sect. B* **2011**, *269*, 1595.
(26) Postawa, Z.; Czerwinski, B.; Szewczyk, M.; Smiley, E. J.; Winograd, N.; Garrison, B. J. *Anal. Chem.* **2003**, *75*, 4402.
(27) Russo, M. F.; Postawa, Z.; Garrison, B. J. *J. Phys. Chem. C* **2009**, *113*, 3270.
(28) Garrison, B. J.; Postawa, Z.; Ryan, K. E.; Vickerman, J. C.; Webb, R. P.; Winograd, N. *Anal. Chem.* **2009**, *81*, 2260.
(29) Baughman, R. H.; Kohler, B. E.; Levy, I. J.; Spangler, C. *Synth. Met.* **1985**, *11*, 37.
(30) *CrystalMaker*; CrystalMaker Software Ltd.: Oxford, England, 1994; www.crystalmaker.com.
(31) Stuart, S. J.; Tutein, A. B.; Harrison, J. A. *J. Chem. Phys.* **2000**, *112*, 6472.
(32) Kelchner, C. L.; Halstead, D. M.; Perkins, L. S.; Wallace, N. M.; DePristo, A. E. *Surf. Sci.* **1994**, *310*, 425.
(33) Chatterjee, R.; Postawa, Z.; Winograd, N.; Garrison, B. J. *J. Phys. Chem. B* **1999**, *103*, 151.
(34) Garrison, B. J.; Postawa, Z. In *Tof-SIMS: Surface Analysis by Mass Spectrometry*, 2nd ed.; Vickerman, J. C., Briggs, D., Eds.; IM Publications: Chichester, U.K., 2012.
(35) Garrison, B. J. In *ToF-SIMS: Surface Analysis by Mass Spectrometry*; Vickerman, J. C., Briggs, D., Eds.; IM Publications: Chichester, U.K., 2001; p 223.
(36) Garrison, B. J.; Kodali, P. B. S.; Srivastava, D. *Chem. Rev.* **1996**, *96*, 1327.
(37) Garrison, B. J.; Srivastava, D. *Annu. Rev. Phys. Chem.* **1995**, *46*, 373.
(38) Brenner, D. W. *Phys. Rev. B: Condens. Matter* **1990**, *42*, 9458.
(39) Brenner, D. W.; Harrison, J. A.; White, C. T.; Colton, R. J. *Thin Solid Films* **1991**, *206*, 220.
(40) Ryan, K. E.; Wojciechowski, I. A.; Garrison, B. J. *J. Phys. Chem. C* **2007**, *111*, 12822.
(41) Delcorte, A.; Garrison, B. J.; Hamraoui, K. *Anal. Chem.* **2009**, *81*, 6676.
(42) Paruch, R.; Rzeznik, L.; Czerwinski, B.; Garrison, B. J.; Winograd, N.; Postawa, Z. *Nucl. Instrum. Methods Phys. Res., Sect. B* **2009**, *267*, 2740.
(43) Krantzman, K. D.; Garrison, B. J. *Nucl. Instrum. Methods Phys. Res., Sect. B* **2009**, *267*, 652.
(44) Delcorte, A.; Restrepo, O. A.; Czerwinski, B.; Garrison, B. J. *Surf. Interface Anal.* **2013**, *45*, 9.
(45) Hamraoui, K.; Delcorte, A. *J. Phys. Chem. C* **2010**, *114*, 5458.
(46) Rzeznik, L.; Paruch, R.; Czerwinski, B.; Garrison, B. J.; Postawa, Z. *Vacuum* **2009**, *83*, S155.
(47) Shinya, T.; Kirihata, H.; Yamaguchi, Y.; Yasumatsu, H.; Kondow, T.; Urbassek, H. M.; Gspann, J. *Nucl. Instrum. Methods Phys. Res., Sect. B* **2009**, *267*, 3080.
(48) Zimmermann, S.; Urbassek, H. M. *Nucl. Instrum. Methods Phys. Res., Sect. B* **2007**, *255*, 208.
(49) Brenes, D. A.; Garrison, B. J.; Winograd, N.; Postawa, Z.; Wucher, A.; Blenkinsopp, P. *J. Phys. Chem. Lett.* **2011**, *2*, 2009.
(50) Delcorte, A.; Garrison, B. J. *J. Phys. Chem. C* **2007**, *111*, 15312.
(51) Cheng, J.; Winograd, N. *Anal. Chem.* **2005**, *77*, 3651.
(52) Paruch, R.; Rzeznik, L.; Russo, M. F.; Garrison, B. J.; Postawa, Z. *J. Phys. Chem. C* **2010**, *114*, 5532.
(53) Garrison, B. J.; Postawa, Z. *Chem. Phys. Lett.* **2011**, *506*, 129.

(54) Rzeznik, L.; Paruch, R.; Garrison, B. J.; Postawa, Z. *Nucl. Instrum. Methods Phys. Res., Sect. B* **2011**, *269*, 1586.
(55) Postawa, Z.; Rzeznik, L.; Paruch, R.; Russo, M. F.; Winograd, N.; Garrison, B. J. *Surf. Interface Anal.* **2011**, *43*, 12.
(56) Paruch, R. J.; Garrison, B. J.; Postawa, Z. *Surf. Interface Anal.* **2013**, *45*, 154.
(57) Paruch, R. J.; Postawa, Z.; Wucher, A.; Garrison, B. J. *J. Phys. Chem. C* **2012**, *116*, 1042.
(58) Paruch, R. J.; Garrison, B. J.; Postawa, Z. *Anal. Chem.* **2012**, *84*, 3010.
(59) Delcorte, A.; Medard, N.; Bertrand, P. *Anal. Chem.* **2002**, *74*, 4955.
(60) Adriaensen, L.; Vangaever, F.; Gijbels, R. *Anal. Chem.* **2004**, *76*, 6777.
(61) Keune, K.; Boon, J. J. *Surf. Interface Anal.* **2004**, *36*, 1620.
(62) Heile, A.; Lipinsky, D.; Wehbe, N.; Delcorte, A.; Bertrand, P.; Felten, A.; Houssiau, L.; Pireaux, J. J.; De, M. R.; Van, R. P.; Van, V. L.; Arlinghaus, H. F. *Surf. Interface Anal.* **2008**, *40*, 538.
(63) Nygren, H.; Johansson, B. R.; Malmberg, P. *Microsc. Res. Tech.* **2005**, *65*, 282.